

Multiscale Analysis of Bamboo Deformation Mechanisms Following NaOH Treatment Using X-ray and Correlative Microscopy

E. Salvati, L.R. Brandt, F. Uzun, H. Zhang, C. Papadaki & A.M. Korsunsky*

MBLEM – University of Oxford, Department of Engineering Science, Parks Road, OX1 3PJ, Oxford, United Kingdom

Contents

Keywords	1
Abstract	2
Graphical Abstract	2
1. Introduction	2
2. Materials and Methods	4
2.1. <i>Material and alkaline pre-treatment</i>	4
2.2. <i>Experimental Synchrotron based Methods</i>	5
2.2.1. <i>In-situ WAXS experiment</i>	6
2.2.2. <i>Crystallinity, Orientation and SAXS</i>	7
2.3. <i>In-situ DIC experiment</i>	7
3. Calculation	7
3.1. <i>Fibre Elastic Moduli</i>	7
4. Analyses and Results	9
4.1. <i>Deformations</i>	9
4.1.1. <i>In-situ WAXS experiment</i>	9
4.1.2. <i>In-situ DIC experiment</i>	10
4.1.3. <i>Elastic properties</i>	11
4.2. <i>Crystallinity, Orientation and SAXS</i>	12
5. Discussions	13
5.1. <i>Deformation Analysis by WAXS technique</i>	13
5.2. <i>Local strain analysis using DIC and elastic properties evaluation</i>	14
5.3. <i>Crystallinity Index and crystal orientation modification</i>	15
5.4. <i>Deformation by SAXS method and general discussion</i>	15
6. Conclusions	15
7. Appendix - Statistical Methods	16
References	18

Keywords

Bamboo, Synchrotron, Alkaline Treatment, Elastic properties change.

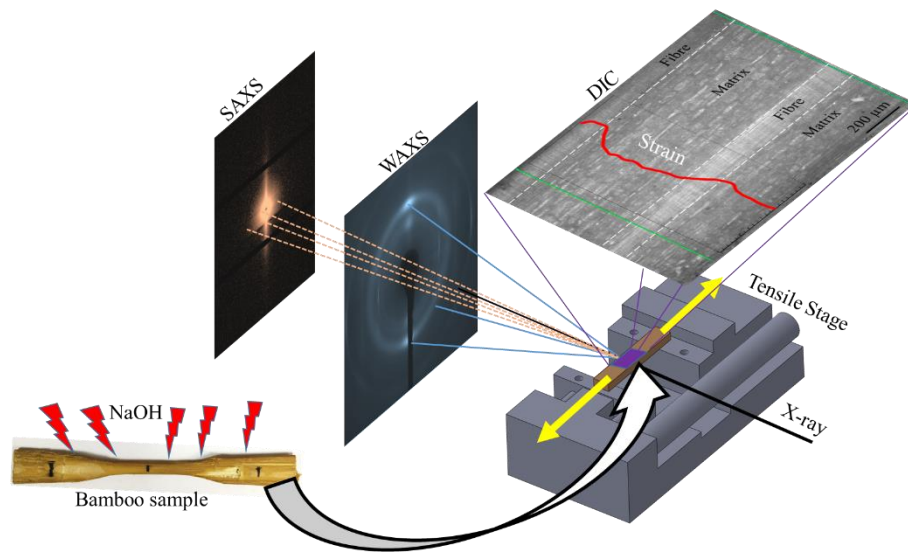
*Corresponding author

E-mail: enrico.salvati@eng.ox.ac.uk; enrico.salvati@outlook.com

Abstract

For hundreds of years, bamboo has been employed for a variety of applications ranging from load-bearing structures to textiles. Thanks to its hierarchical structure that is functionally graded and naturally optimised, bamboo displays a variation in properties across its stem that ensures exceptional flexural performance. Often, alkaline solutions are employed for the treatment of bamboo in order to alter its natural elastic behaviour and make it suitable for particular applications. In this work we study the effect of NaOH solutions of five different concentration (up to 25%) on the elastic properties of bamboo. By exploiting the capabilities of modern experimental techniques such as *in situ* synchrotron X-ray scattering and Digital Image Correlation, we present detailed analysis of the deformation mechanisms taking place in the main constituents of bamboo, i.e. fibres and matrix (Parenchyma). The principal achievement of this study is the elucidation of the deformation mechanisms at the fibre scale, where the relative sliding of fibrils plays a crucial role in the property modification of the whole bamboo stem. Furthermore, we shed light on the parenchyma toughness variation as a consequence of alkali treatments.

Graphical Abstract



1. Introduction

In common with many biological materials such as bone, wood, tooth and nacre, bamboo has a hierarchical structure that extends from the macroscopic level all the way down to the molecular scale [1]. Particularly for structural applications, bamboo has been widely employed to fabricate mechanical elements and structures [2, 3] and also as a reinforcement in polymers or concrete [4-6]. Since bamboo is a rapid renewable and sustainable resource at low cost, it plays a relevant role in building greener economies.

For hundreds years [7], bamboo has enjoyed a vast and varied range of applications thanks to its structure that is functionally graded and naturally optimised to obtain a ‘smart’ variation in properties across its stem [8]. As shown in Figure 1, such variation is accomplished by the presence of non-uniformly distributed longitudinal fibres, with higher density at the outer wall [7]. This makes the outer surface stronger than the inner surface and results in a remarkable performance concerning stiffness and strength properties. Conversely, the density of the bamboo matrix (*Parenchyma cells*) is higher at the inner region of the bamboo culm [9, 10]. As the position across the culm diameter varies, the fibres change in shape; almost circular at the outer periphery and elliptical or separated into four parts at the inner region. As far as the parenchyma constituent is concerned, its primary task is to store nutrients and, due to its hollow structure, reduces the overall density of the bamboo. However, it has been seen that at the micro-/nano-scale the parenchyma is itself constituted by nano-fibrils of the same type of those found in the fibres [11].

As just mentioned, at the microscopic scale the characteristic reinforcing elements that can be found in the bamboo stem are the fibres. Bamboo fibres are composed of a number of fibrils with size in the range of 10-20µm, separated from each other by a thin wall of matrix. This 1-5µm thick layer is mainly made of lignin and

hemicellulose [12, 13], and organised in a honeycomb-like manner. This fibrils arrangement makes the fibre itself a composite material in which the lignin and hemicellulose play an important role in attaining the characteristic properties of bamboo.

A further close up into the microstructure of a single fibril shows its nano-scale composition and organisation. It has been seen that a single fibril contains straggled and twisted elongated cellulose elements, resembling the classic metal ropes formed by many twisted wires. Such particular nano-scale organisation of cellulose elements is in part responsible for the excellent bending properties of the single fibre and hence of the whole bamboo composite [10]. It is also worth highlighting the polycrystalline structure of the single cellulose fibril, which was found to contain polygonal nanograins with diameters in the range of ~20-200nm [14].

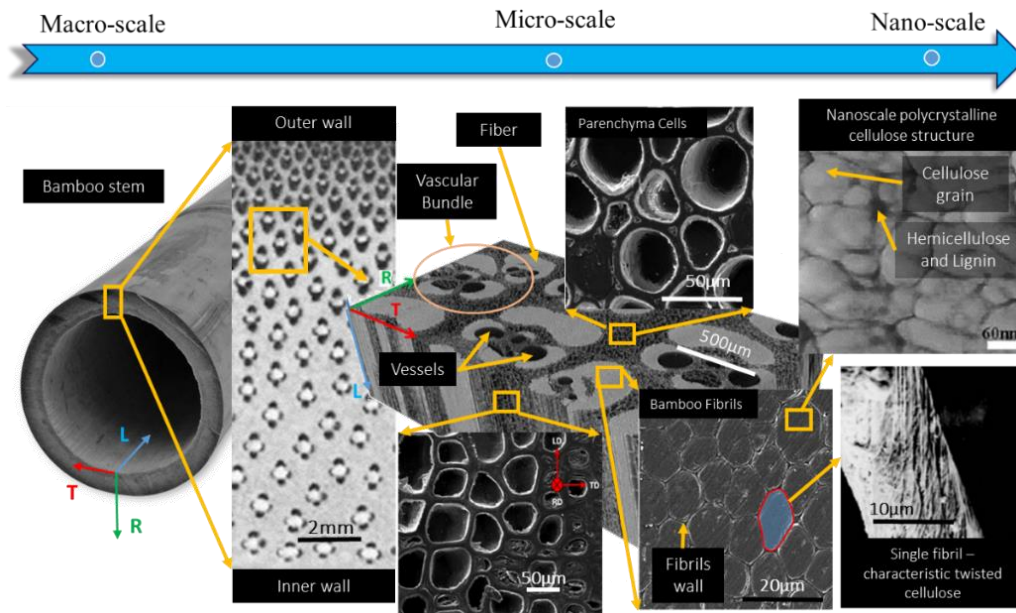


Figure 1 Bamboo hierarchical structure. A composition of optical, SEM and AFM images from [7, 10, 15, 16]

As far as the mechanical properties are concerned, contrasting behaviour can be found within a bamboo culm. Indeed, individual bamboo's fibres may reach a strength of up to ~900MPa, whilst the matrix can only resist stresses 12 times lower (~50MPa). Similarly, a considerable mismatch can also be observed concerning the elastic properties, in fact fibres show stiffer behaviour than the matrix, respectively ~50GPa and 2-7GPa in terms of Young's modulus [17-19]. Also, the graded structure in terms of the vascular bundles shapes across the culm cross-section is reflected in the mechanical properties of the single bundle. In fact, whilst the fibres show same properties, the vascular bundle assembly shows stiffer and stronger behaviour at the outer part of the culm (~2 times higher) [18, 20].

Today, bamboo is employed in a wide range of applications mostly thanks to the pre-treatments processes applied to the material in order to change its mechanical and chemical properties. The most widespread technique involves the use of alkaline solutions, classically NaOH, which reacts primarily with the matrix of the bamboo composite. It has been shown that a weaker matrix can be removed by alkali treatment with little effect on the fibres, when the concentration of NaOH is lower than 10%. At higher concentrations, e.g. 20 or 30% NaOH, the solution dissolves a substantial part of the lignocellulosic constituent that holds together the fibrils. For this reason, wherever the bamboo fibres are used as reinforcements in polymeric composites, bamboo should be treated with alkali solution of approximately 10% strength to remove only low strength bamboo matrix [10]. This process also improves the fibres wetting ability with a consequent enhancement of the fibre-matrix adhesion when used as reinforcements [21].

Bamboo is also frequently used in the textile industry. Clearly, the production of textile objects requires the bamboo materials to be a softer than the pristine condition. With this purpose, alkaline treatments are frequently employed for the modification of those elastic properties.

As concerns alternative energies sources, bamboo may also be considered a good candidate as a replacement of petroleum-based fuels [22, 23]. In case the source of biomass is cellulose-based (e.g. wood, bamboo), the extraction of the combustible can be efficiently performed through a pre-treatment procedure that enables the removal (or reduction) of the lignin hemicellulose and silica, which in turns considerably improve the hydrolysis process [24]. Amongst all the pre-treatment techniques, interestingly the use of NaOH alkaline solutions has raised a relevant interest by the scientific community [14, 25-28].

The present work aims at shedding some light onto the mechanisms that are responsible for elastic properties modification when alkaline solution is applied to bamboo culms. To accomplish this task, we tested a series of bamboo specimens treated with NaOH solutions at various concentrations. By exploiting the capabilities of Synchrotron-based X-ray techniques, such as Wide/Small Angle X-ray Scattering (WAXS & SAXS), in-situ tensile test experiments were performed in order to monitor the material mechanical response of both the whole “composite bamboo” and its fibrous content. As seen in previous works, this experimental setup is suitable for the analysis of multi-constituent materials, mainly in those showing crystalline structure [29, 30]. The combination of SAXS and WAXS techniques has also been used for the in-situ study of materials deformation across the length-scales [31-34]. Since the WAXS technique is able to provide accurate assessment of the deformations occurring in crystalline constituents at the crystal lattice scale, and the bamboo cellulose fibres are known to exhibit a crystalline structure, we employed this method to attempt monitoring the bamboo fibres elastic deformation evolution during the tensile tests.

In addition, a coupled in-situ Optical Microscopy (OM) and Digital Image Correlation (DIC) analysis was carried out during the tensile test of three selected samples, namely the untreated and those treated with 20% and 25% NaOH solution. A new set of samples was used for this experiment; this strategy was also aimed at verifying the repeatability of the results, which could then be compared to the results obtained through the Synchrotron-based techniques. The purpose of this analysis was the evaluation of the deformation taking place at the micron scale; i.e. the relative movements of the fibrils and parenchyma cells. At the same time, the volume fraction of fibres is assessed by analysing images of the specimen’s cross-section. In this way, the effective stress acting along the fibres is computed and a discrimination between the elastic properties of the whole composite and the fibres is performed. Since the bamboo is a composite containing parallel and aligned reinforcing fibres, the elastic properties of the matrix can be promptly calculated. Further useful insights are extracted from these data, such as the degree of crystallinity and the preferential orientation of the nanograins in the fibres. On the other hand, the SAXS configuration enables the study of material structures lying within a range of dimensions in the order of tenth of nanometres. Although, the abstraction of quantitative deformation information is rather challenging using this technique, qualitative evidence of deformation evolution is analysed and discussed.

2. Materials and Methods

2.1. Material and alkaline pre-treatment

The bamboo specimens were machined from culms of the *Bambusa Glaucescens* type, also known as “Golden Goddess”. The age of the used bamboo was estimated to be >2 years, therefore in the stage of its life where the maturity is reached and the layering structure of the fibre bundle does not vary as the bamboo keeps growing [35]. As shown in Figure 2, a classic dog-bone geometry was adopted for the in-situ tensile testing. The thickness t and the width w of the resistant cross-section ranged respectively between 1.15-1.25mm and 2-2.4mm. In order to reduce the bending effect due to the clamping over concave and convex surfaces, the sample’s extremities were flattened by material removal.

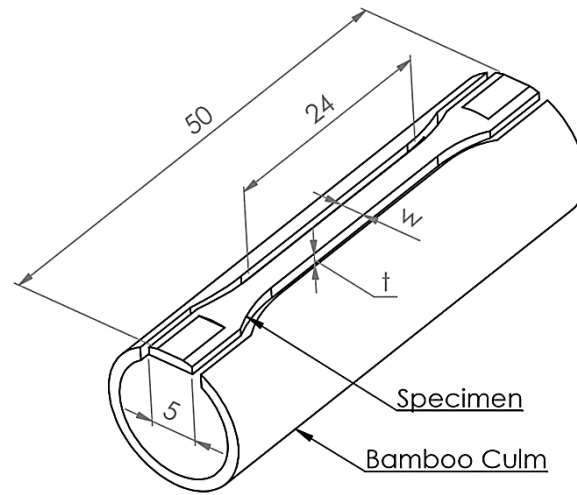


Figure 2 Sample geometry and principal dimensions (dimensions in millimetres).

The alkaline pre-treatment was conducted using NaOH at various concentrations, as listed in the Table 1. The samples were submerged into the solution for 20 minutes and the tensile test started at around one hour after the end of the sample treatment. All the tests were performed at room temperature and the ambient relative humidity levels were maintained between 45% and 55%.

Sample Designation	Concentration of NaOH [%]
0	0 (Untreated)
1	5
2	10
3	15
4	20
5	25

Table 1 Samples

2.2. Experimental Synchrotron based Methods

The in-situ experiment was performed at beamline B16 at the synchrotron facility Diamond Light Source (DLS), Harwell (UK). The tensile load was applied to the samples using a Microtest deformation stage by Deben Research (UK), capable of applying up to 5kN of force. A schematic illustration of the setup layout and distances is shown in Figure 3. The test was run by precisely controlling the displacement of the rig crosshead and the applied strain rate was $\dot{\epsilon} = 5 \times 10^{-5} \text{ s}^{-1}$. The tensile stage was mounted onto two translation stages that allowed the localisation of the sample with the respect of the X-ray beam spot, respectively along x and y directions accordingly to Figure 3. The identification of the region of interest was facilitated by using an imaging detector (“X-ray eye”) sCMOS in transmission mode.

Regarding the in-situ SAXS/WAXS experiment, a monochromatic beam with a photon energy of 15keV was employed. A beam spot size of 0.5x0.5mm was achieved by cropping the main beam with mechanical slits. On the other hand, the radial scan of the bamboo culm was conducted using a focussed X-ray beam by using a Compound Refractive Lens (CRL) focussing device which permitted to achieve a beam spot size of few microns in size, at the focus point. Although the X-ray beam divergence was relatively small, it was not possible to acquire the SAXS patterns along the radial direction, as at the long distance the direct beam overlapped the diffraction pattern. Where possible, the SAXS diffraction patterns were acquired by a Pilatus detector, while an ImageStar 900 detector was employed for the acquisition of WAXS patterns. At each loading step, SAXS and WAXS detectors were alternately placed in transmission to acquire the respective patterns.

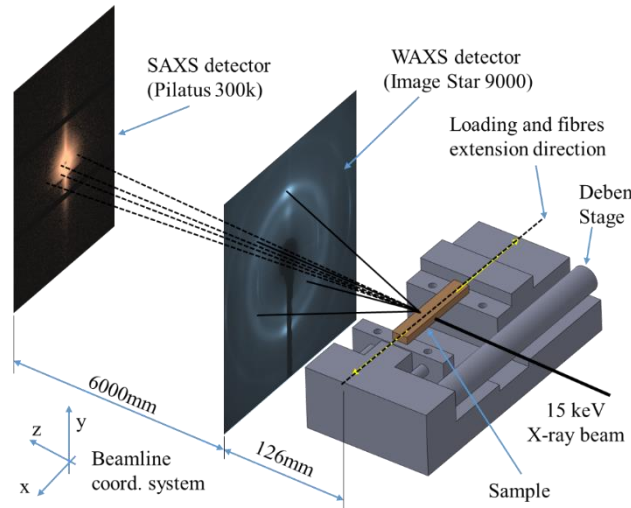


Figure 3 Synchrotron SAXS/WAXS experimental setup

Precise calibration of the sample-detector distances, mandatory for a correct definition of the scanned q -range, was done employing standard Silicon powder (NIST SRM 640d) and Lanthanum Hexaboride (LaB₆, NIST SRM 660a), concerning the WAXS detector distance. While SAXS calibration was obtained using dry collagen chicken [36].

SAXS and WAXS diffraction patterns were interpreted using Fit2D software. This allowed the extraction of 1-D profiles as a result of the azimuthal integrations at the chosen angular range, as a function of the 2-theta diffraction angle.

In order to determine the actual stress state present in the fibres during loading, knowledge of the two composites phase area ratio was required. This task could be promptly accomplished by analysing the samples cross-sections. The post-mortem evaluation of the fibre area ratio with respect to the whole sample cross-section area was performed by cutting the tested samples and observing the bamboo structure using an optical microscope. The observed surface was polished using 800 and 1200 grade grinding papers. As seen in other works [37], the analysis of the images collected by microscopy techniques is able to reveal the bamboo fibres thanks to its enhanced contrast with the matrix, therefore the fibres area fraction was evaluated by exploiting some image intensity thresholding capabilities of the ImageJ software.

2.2.1. In-situ WAXS experiment

Since the bamboo can be thought of as a composite material, the stresses that the material needs to withstand during tensile test is not uniformly distributed through the sample, even in the simple case of an un-notched sample. It is then evident that a sole macroscopic approach to the problem would fail in capturing the stress and strain gradients taking place during linear deformation.

The whole set of samples described in Table 1 was tested in displacement control and simultaneously, the macroscopic stresses and strains arising were thoroughly monitored, up to the rupture of the sample. Whilst the samples were loaded, WAXS diffraction patterns were continuously acquired. Examples of acquired WAXS patterns at the unloaded condition are shown in the Figure 4. These patterns show the typical Debye-Scherrer rings, which are associated to certain crystalline plane reflections; the relevant planes were identified and labelled in Figure.

Amongst the number of information that can be extracted from the analysis of these patterns, we focus our effort in the analysis of strains. It is well known that the radial position of rings is associated with the interplanar distance and therefore, under loading condition, variation of this distance can be correlated to the strain occurring at the crystalline scale [38-44]. For a given Miller index hkl , the conversion between the interplanar distance (lattice parameter d_{hkl}) and the estimated lattice strain ϵ_{hkl} is given by:

$$\varepsilon_{hkl} = \frac{d_{hkl} - d_{hkl}^0}{d_{hkl}^0} \quad (1)$$

where d_{hkl}^0 is the lattice parameter corresponding to the unstrained state.

2.2.2. Crystallinity, Orientation and SAXS

An important aspect that is surely worth investigating is the Crystallinity Index (CI) evolution as the bamboo is treated with alkaline solution. Adopting the same deconvolution strategy seen in the previous section, this task can be accomplished using the amorphous subtraction method in an accurate manner [45]. This method relies on the use of the deconvolved peak intensities:

$$CI = \frac{I_{200} - I_{AM}}{I_{200}} \quad (2)$$

where I_{200} is the intensity of the $\langle 200 \rangle$ peak, labelled #5 in Figure 5, and I_{AM} is the intensity of the amorphous broad peak that was in turn deconvolved. At the unloaded sample state, the CI trend is reported in Figure 10(a).

As the alkaline solution is applied to the samples, the preferential orientation of the crystals in the material may change and play an important role in the elastic response of the composite. In this study the analysis of the preferential orientation modification as the solution was applied was carried out by simply comparing the peak intensities at two orthogonal directions $I_{0^\circ,i}$ and $I_{90^\circ,i}$, respectively at $\alpha=0^\circ$ and 90° according to the scheme in Figure 4. Therefore, we analysed the Preferred Orientation Index (POI), normalised by its value at the untreated condition as follows:

$$POI_i = \left(\frac{I_{0^\circ,i}}{I_{90^\circ,i}} \right) / \left(\frac{I_{0^\circ,0}}{I_{90^\circ,0}} \right) \quad (3)$$

2.3. In-situ DIC experiment

A convenient way of analysing the total deformation gradients taking place in the bamboo material is by using the DIC technique. This technique relies on the displacement tracking of fine features present on the sample surface during loading. Provided that the surface presents such characteristic appearance, a successful DIC analysis leads to the evaluation of the surface displacement field and, after apposite calculations, to the strain field. In this study we utilised a freeware software based on Matlab which allowed manipulation of raw data as required [46].

The analysis of displacements and strain at the micro-scale is conducted employing the DIC technique. The in-situ acquisition of the images was performed by using an Alicona InfiniteFocus optical microscope which provided $\sim 2\mu\text{m}$ lateral resolution and accurate focus ensured by the out-of-plane scan reconstruction implemented in its dedicated software. The samples surfaces were prepared again using the same process as mentioned before, for the preparation of cross-sections. The region of interest was chosen sufficiently large in order to capture displacements occurring both in the fibre and parenchyma regions. As well as the in-situ WAXS experiment, the strain rate applied was $\dot{\varepsilon} = 5 \times 10^{-5} \text{ s}^{-1}$. Differently, in this case holding the sample at constant load was required to enable the capture of the image. The total time necessary to accomplish this task was ~ 1.5 minutes.

3. Calculation

3.1. Fibre Elastic Moduli

With the purpose of fully characterising the elastic behaviour of the bamboo fibres, we employ the rule-of-mixture. This rule is usually used to estimate the average composite mechanical and physical properties along different directions.

The actual stress-strain relationship describing the elastic properties of the fibres can only be evaluated upon correct assessment of the fibre area fraction A_f within the bamboo cross-section. A convenient way of representing this fraction is through the ratio area fibres vs. area matrix, φ_f . φ_f is the fibre volume fraction defined as $\varphi_f = A_f/A_m$, where A_f and A_m are respectively the sample cross-section area corresponding to the fibres and area covered by the bamboo matrix (parenchyma) excluding the vascular vessels, which are supposed to be hollow. These parameters were evaluated by analysing optical images of the sample cross-sections using ImageJ software. Same calculation was confidently employed in the past by other researchers [47].

In this material, the fibres can be seen as a reinforcement, aligned with the loading direction and embedded in a matrix. Due to the specific sample length-scale, the fibres can be considered continuous along the longitudinal direction and therefore the strains occurring in the sample can be thought as constant through the cross-section, assuming the same magnitude in both the fibres and matrix. In any case, the correctness of this assumption is verified and shown in the following section of the paper dedicated to the DIC analysis. According to the rule-of-mixture, the Young's modulus of a composite can be calculated by using

$$E_c = k E_f \varphi_f + E_m(1 - \varphi_f) \quad (4)$$

where E_c , E_f and E_m represent respectively the Young's moduli of the whole composite, of the fibres and of the matrix. While the parameter k is the fibre efficiency that takes into account the fibre length in case they are not continuous. However, in this study we assume that the fibres run along the entire samples length and therefore the parameter is assumed to be equal to 1.

It is then obvious that the evaluation of the fibres elastic modulus can be performed only upon knowledge of the matrix characteristics. However, it is important to notice that matrix and fibres show a large discrepancy in terms of elastic properties, as discussed in the introduction. In fact it can be surmised that the ratio between these constituents of the composite lies in the range: $7 < \left(\beta = \frac{E_f}{E_m}\right) < 25$. By assuming that this ratio is also valid in the present study, the determination of the fibre elastic modulus can be determined. It is important to report that in terms of elastic modulus, values of β at the lower or upper limits led to change in the calculated elastic modulus in the order of 8%. This additional source of error is accounted in the error propagation calculation.

By substituting the definition of E_m as a function of β into the eq.(4) we can then make the calculation of E_f explicit:

$$E_f = \frac{E_c}{k \varphi_f + \frac{(1 - \varphi_f)}{\beta}} \quad (5)$$

The elastic modulus of the composite was computed by fitting the stress-strain curves with a linear regression and extracting the resulting slope. As far as the elastic moduli ratio β , this was assumed to be equal to an averaged value between the range provided by literature, therefore $\beta=16$.

For this study, thorough accounting of the several sources of errors was conducted and calculated using the error propagation theory. Ranging from the sample dimensions errors to the fitting accuracy of the XRD peaks and DIC tracking errors, these inaccuracies were accurately summed to obtain a global assessment of the measurement errors in the quantification of the elastic properties.

4. Analyses and Results

4.1. Deformations

4.1.1. In-situ WAXS experiment

In order to capture the sole longitudinal component of elastic strain, the peak shifting analysis is performed by computing an azimuthal integration of $\pm 15^\circ$ around the direction corresponding to the sought component of strain, according with the region contoured by the red lines in Figure 4. In this figure, the longitudinal component of strain corresponds to the x -axis and therefore, the azimuthal integration is done within $\alpha \pm 15^\circ$.

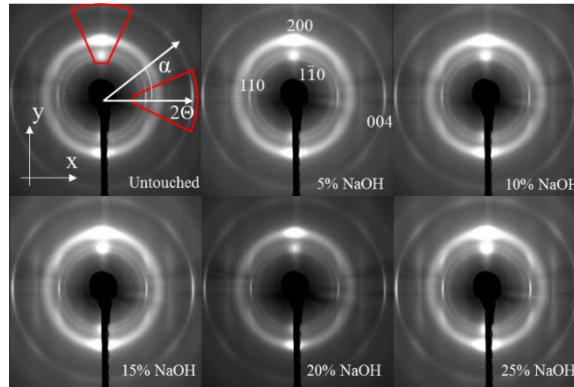


Figure 4 WAXS diffraction patterns and integration regions

After the identification process of the relevant peaks, a deconvolution of the individual peaks contribution was performed on the 1D diffraction patterns; examples are given in Figure 5(a). This deconvolution firstly involves subtracting the X-ray background and the contribution given by the amorphous portion of material, secondly, iteratively it finds the contribution of each peak to the construction of the actual diffraction spectra. In addition to this analysis, we report in Figure 5(a) some diffraction spectra collected in a sample configuration corresponding to the fibres being parallel to the x-ray beam. The patterns were collected by performing a bamboo culm radial raster scan.

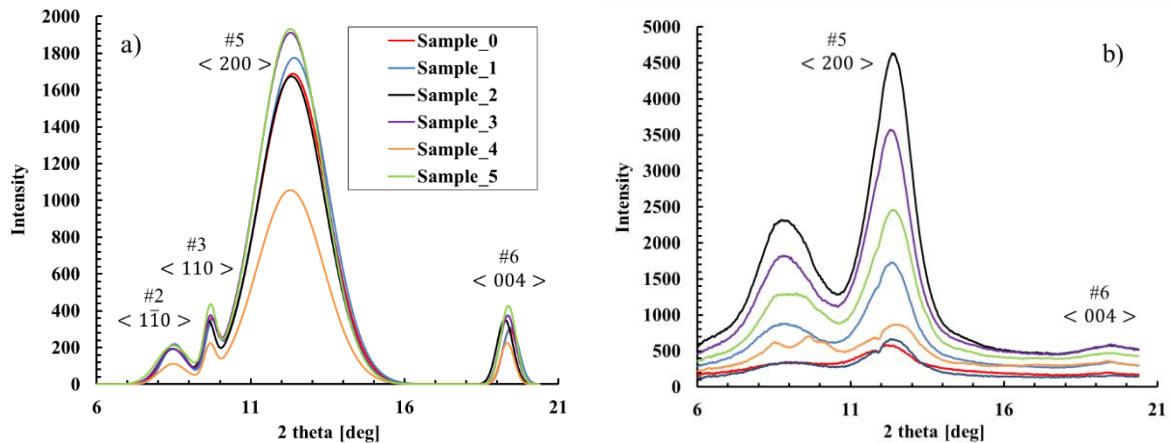


Figure 5 XRD profiles. (a) Highlight of the significant cellulose WAXS diffraction peaks obtained by spectra deconvolution. The diffraction pattern was obtained in the sample configuration depicted in Figure 3. b) Diffraction patterns obtained by aligning the bamboo fibre with the z -direction shown in Figure 3.

It is worth highlighting that the diffraction images show a characteristic texturised patterns which are clearly associated with a preferential orientation assumed by the crystals in the material. This preferential orientation is very likely to be associated to the longitudinal evolution of the cellulose fibres which are of ordered nano-crystalline nature. Therefore, we assume that the strain monitored by the XRD technique using the strong reflections from the ordered crystalline structures is primarily the result of the deformation occurring at the crystalline scale in the bamboo fibres. As exhaustively reported in the literature [48, 49], the crystalline plane

$\langle 004 \rangle$ is oriented normally to the longitudinal direction of the fibre, therefore only detectable when such plane is parallel or close to the x-ray beam. In fact, as it can be observed in Figure 5(b), when the x-ray is approximately aligned with the fibre longitudinal direction, the plane $\langle 004 \rangle$ does not generate any reflection.

With the purpose of monitoring the elastic strain predominantly occurring in the fibres during loading of the samples, the displacement of peak #6 corresponding to the plane $\langle 004 \rangle$ was analysed. Such choice was driven primarily by the fact that along the direction of interest (x-axis) this peak shows strong intensity and therefore likely to be associated to the preferential orientation present in the fibres. In any case, the strain analysis was also performed using the peak #5 and, as expected the scatter of those is higher because it includes also the contribution of less ordered cellulose components, such the parenchyma (matrix) [11].

The plots collected in Figure 6 present the stress-strain curves of the tested samples. It is worth highlighting that the stress-strain response shown in Figure 6 refers to a resistant cross-section equivalent to the entire sample area, the whole composite.

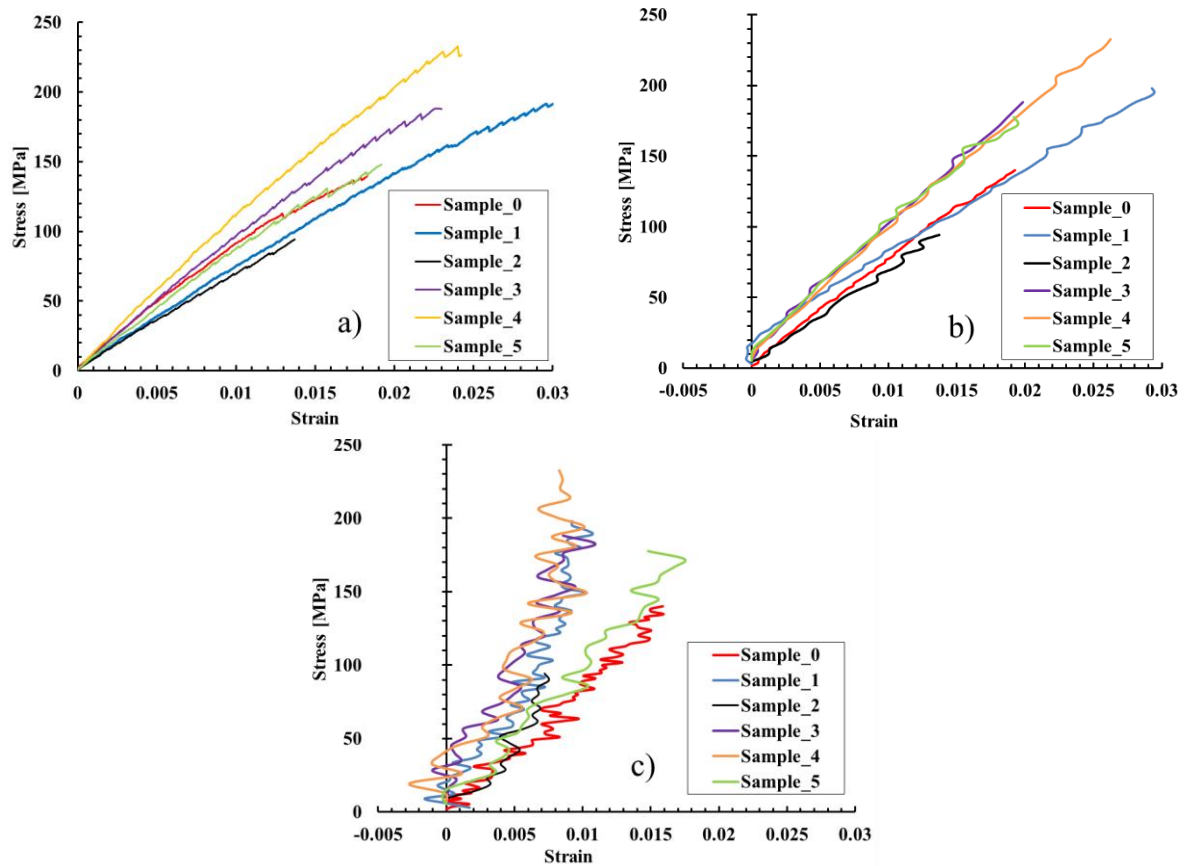


Figure 6 Tensile test results: Stress-Strain curves. (a) Macroscopic (Tensile stage). (b) Fibres behaviour from Peak #6. (c) Cellulose constituents from Peak #5.

4.1.2. In-situ DIC experiment

This experiment was carried out using a new set of bamboo samples, which were treated in the same manner as described for the in-situ Synchrotron experiment. Images of the sample surface were acquired at several loading stages in order to capture the strain evolution and evaluate the elastic properties. According to Figure 7, two parallel and 1.2mm spaced lines of tracking markers were placed perpendicularly to the loading direction. This allowed capturing the fine displacements gradients across the fibres, matrix and interfaces.

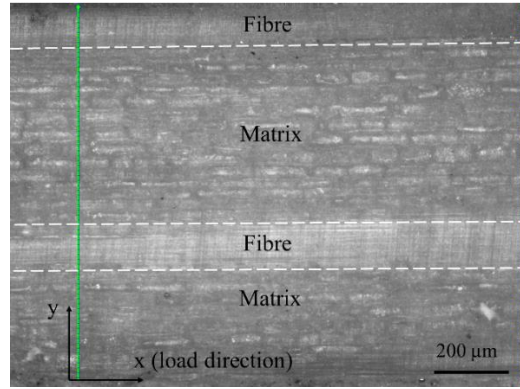


Figure 7 Example of optical image of bamboo polished surface showing the fibres and matrix constituents (20% NaOH). The fine green dotted lines indicate the DIC markers position.

A collection of strain profiles across the sample width as the external load increased is shown in Figure 8. Particularly, Figure 8(a) refers to the untreated sample and Figure 8(b) and Figure 8(c) respectively to the samples treated with 20% and 25% NaOH solution. With the purpose of facilitating the comprehension of the plots, the backgrounds of the regions is coloured according to the constituent of the bamboo (i.e. fibre in yellow and matrix in green).

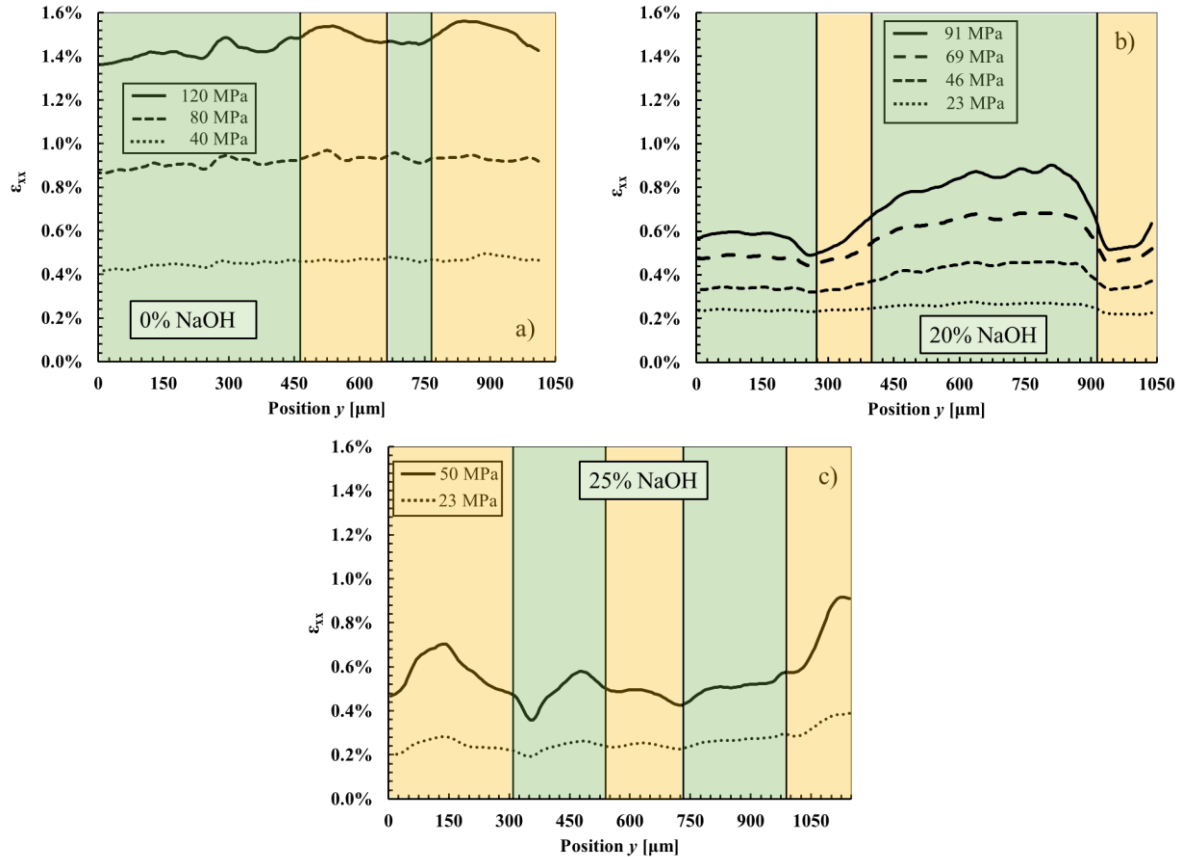


Figure 8 DIC Strain distribution along the sample cross section at several loading levels. (a) Untreated sample, (b) 20% NaOH treated sample and (c) 25% NaOH treated sample. The green regions correspond to the matrix while the yellow regions are associated with the fibre domains. The stress levels refer to the entire sample cross section area (matrix + fibre).

4.1.3. Elastic properties

Figure 9 reports three relevant elastic moduli of the analysed bamboo at different alkalinity percentage namely, composite, fibres and matrix. Each evaluated point comes with the associated error bar representing the 95% confidence interval.

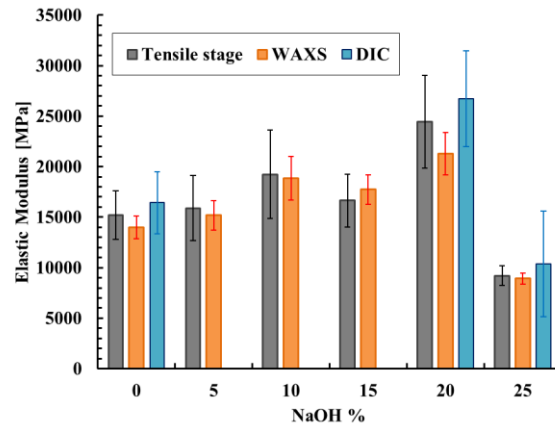


Figure 9 Evaluated elastic moduli of the fibres at different NaOH concentrations using different techniques.

4.2. Crystallinity, Orientation and SAXS

The POI was calculated by using the intensity of the two principal peaks previously involved in the strain analysis, #5 and #6. The results are summarised in the plot in Figure 10(b).

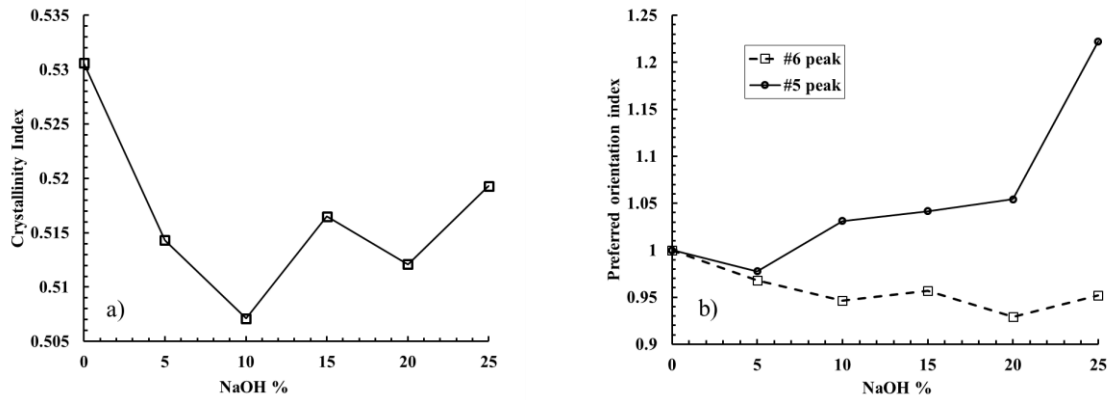


Figure 10 Intensity derived plots. (a) Crystallinity index and (b) Preferred Orientation Index

Analysis of the SAXS pattern is usually conducted with the goal of retrieving information about structures in the material ranging from few to tens of nanometres in size. As shown in Figure 3, the typical SAXS pattern obtained from the exposure of bamboo to X-ray shows a strong diffraction band aligned perpendicularly to the fibres longitudinal extent. This demonstrated how features of this length scale are somehow preferentially oriented.

An example of azimuthal integration of $\pm 15^\circ$ around the direction aligned to the fibre longitudinal direction is shown in Figure 11(a). As it is possible to observe from the log-log plot, a pseudo-linear decay is present in this region. More precisely, the scattering intensity decay is proportional to q^{-4} , indicating that the scatter can be imputed to any system or structure with sharp or smooth surface. Furthermore, no information related to the size of these structures could be retrieved since there are not peaks associated to a particular predominant size. It is also worth highlighting that the peak $\sim 0.11 \text{ nm}^{-1}$ is only due to the presence of the x-ray beam stop, which abruptly cuts the intensity of the scatter.

On the other hand, some insight into the presence and multiplication of these systems could be obtained from the evaluation of the SAXS intensity as the sample was loaded. Figure 11(b) reports the intensity change experienced during the in-situ tests, referred to the unstrained condition.

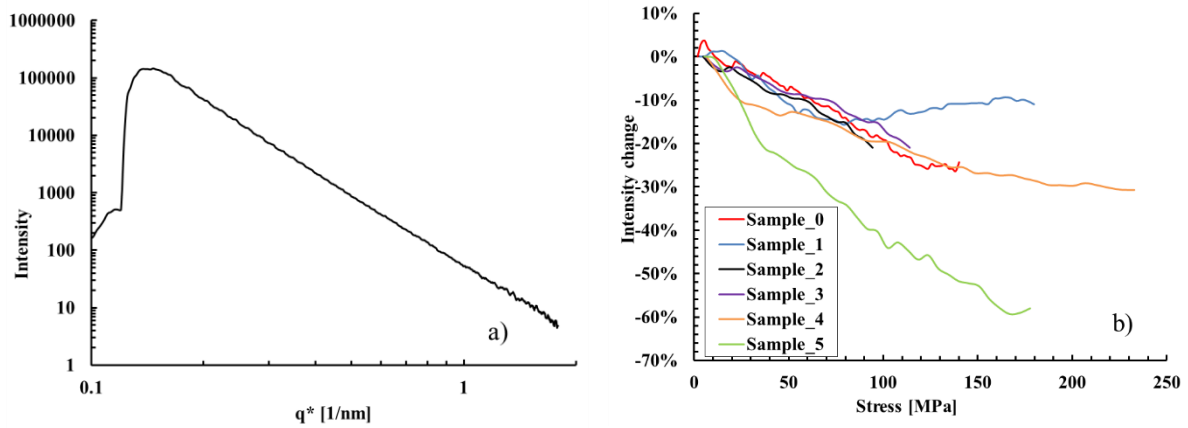


Figure 11 SAXS derived plots. (a) Intensity plot at low q -range and (b) Intensity change during tensile test

5. Discussions

Detailed analysis of the deformation mechanisms has been conducted and presented in this manuscript. Three complementary techniques, namely micro tensile stage, WAXS and DIC, were employed for the study of material elastic properties, primarily regarding the reinforcing component of the bamboo, the fibres.

5.1. Deformation Analysis by WAXS technique

While the tensile stage provided the macroscopic stress strain response, the WAXS technique was able to capture deformations taking place in well-defined classes of crystal structures. As it is possible to observe from the collection of stress-strain responses obtained from macroscopic observation and WAXS analysis reported in Figure 6, wherever the reflection peak associated with the crystal plane $\langle 004 \rangle$ (named as #6) is used for the strain analysis, a close match with the macroscopic response is experienced. This is an evidence that the deformation obtained from this peak is related to the driving deformation component within the bamboo, which undoubtedly is the fibre. Further evidence can be found in the strong preferential orientation manifested by this peak, as shown in Figure 4, where strong diffraction intensity can be observed in the direction parallel to the fibre elongation direction, x . This indicates that the nano-crystalline structure existing in the fibrils shows high degree of alignment of the grains. On the other hand, different behaviour can be perceived when the broadest peak is used for the evaluation of the deformations occurring in the bamboo, i.e. $\langle 200 \rangle$ named #5. Indeed, a much higher degree of data scatter was obtained and globally, low magnitudes of deformations were obtained (Figure 6(c)). As well as the peak $\langle 004 \rangle$, the azimuthal integration was performed around the loading direction but in this case, the preferential orientation was located at a perpendicular direction. Therefore, the amount of deformation measured is the outcome of a more disordered system, which we strongly believe is linked to the cellular structure of the bamboo matrix. As far as the lower magnitudes of strain are concerned, this can be explained by the fact that the bamboo matrix is generally weaker than the fibre as explained in the introduction, leading to a premature fracture and a consequent global reduction in the strains. This is clearly visible from the constant strain measured in these samples when external load exceeds ~ 100 MPa (Figure 6(c)). An illustration of crack propagating through the matrix, whilst the fibre is not fractured, is given in Figure 12(a); this fracturing mechanism is responsible for the remarkable fracture toughness of bamboo [15]. It is worth noting that the deformations taking place in the samples treated with high alkalinity solutions (i.e. 25%) and the untreated material, turned out to be close to the magnitude of macroscopic response and WAXS. This behaviour suggests that in the first instance the low alkaline solution reduces the strength of the bamboo matrix, while the 25% NaOH solution brings the matrix strength back to its original strength.

5.2. Local strain analysis using DIC and elastic properties evaluation

Further lights onto the deformation behaviour of the fibres and matrix was shed by using the DIC technique. Concerning this type of analysis, two alkaline treatments were applied to the samples, at the most relevant percentage, namely 20% and 25%. In the first instance it is important to make some observations regarding the strains occurring in a single fibre. As shown in the Figure 8, the single fibre is generally not uniformly strained. This effect is due to the relative movements of the fibrils that are present in the fibre and it can be a good qualitative index of the shear load that the fibre can withstand. For instance, the sample treated with 20% NaOH solution shows high degree of strain variability within a single fibre, up to $\Delta\epsilon \sim 0.4\%$. Whilst both the untreated sample and the one treated with 20% NaOH present much smaller strain change. Apparently, above a certain % of NaOH the adhesion effectiveness between fibrils decays. It is well-known that the alkaline solution is effective in breaking the lignin sealing that lies between fibrils [24, 50, 51] and, for higher concentrations it also disrupt the crystalline structure of the fibrils. Same behaviour has been observed in a number of biomaterials containing fibrils bonded by hemicellulose and lignin [50, 51]. Moreover, as seen in a study dealing with the stress relaxation induced by NaOH solutions [51], the disruption of these lignin chains implies an enhanced mobility of the composite constituents at this scale, with a consequent relaxation of internal residual stress.

This explains why at 25% NaOH a large variation of strain is experienced in the fibre. Later, it will be discussed how this has an effect on the elastic property. Further comments can be drawn concerning the deformations taking place in the bamboo matrix, which are strictly connected to the strain behaviour observed in the WAXS strain analysis of the disordered structures; peak $\langle 200 \rangle$. In fact, the sample treated with 20% NaOH displays considerable difference in terms of strain in the two matrix regions which may be related to the presence of crack propagating and the visible deformation is due substantially by the adhesion with the neighbouring fibres.

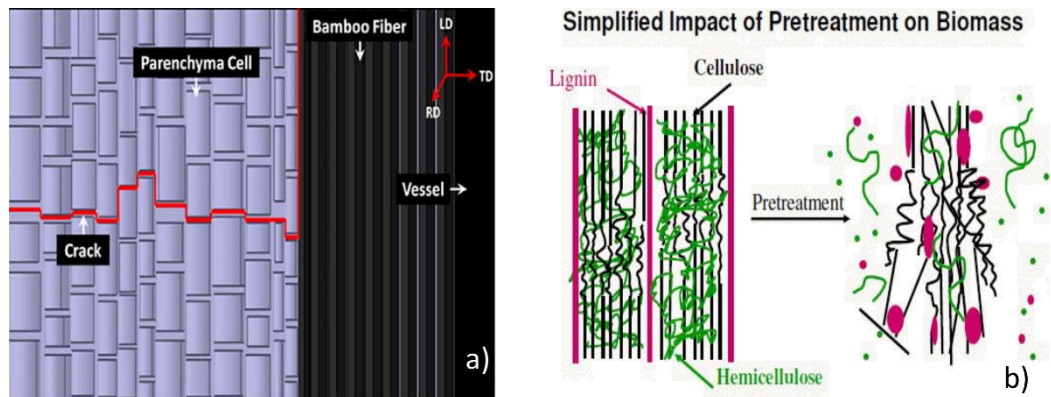


Figure 12 (a) Crack path associated with the softer matter in the parenchyma [15] and (b) effect of pretreatment in fibres [24]

Due to the composite-like nature of the bamboo, when studying the mechanical properties, attention must be paid to the behaviour of the most relevant constituent. As shown before, the calculation of the elastic properties is based on the assumption that the bamboo fibres are much stiffer than the neighbouring matrix by a factor of 16. Thanks to this assumption, it was possible to evaluate the elastic modulus of the fibres at several alkalinities of the chemical treatment. Such assumption was justified by the adequate evidence provided by literature and, however, the statistical variation of this ratio was accounted for through accurate error propagation calculation. In addition, the amount of fibrous matter compared with the matrix was assessed by optical technique for each tested sample and, again, measurements error accounted. The outcome of this calculation framework is reported in Figure 9. Clearly, a modification of the fibres elastic property was experienced as shown in Figure 9 and an evident trend can be perceived. In detail, a gradual increment of the fibres elastic modulus was revealed as the degree of alkalinity is increased, reaching the maximum value at 20% NaOH. Conversely, when a 25% NaOH solution was applied to the sample the Young's modulus underwent to a sudden drop of around half the magnitude of the 20% NaOH treated sample. Same type of elastic modulus trend is reported in the literature, although concerning the overall response of the bamboo and not the sole fibres [52]. Therefore, quantitative comparison between the results cannot be made since the fibre volume fraction is not provided in the relevant literature.

Same effect was seen when bamboo is used as reinforcing element in composites [21]. It is worth noting, that the evaluated elastic modulus using three different techniques provided very satisfactory consistency, despite for the case of DIC analysis a different set of samples was used. It is important to highlight that the bamboo is a hydrophilic material which one might think the elastic properties can be affected by the water content. Nevertheless, it has been seen experimentally that even after long exposure to water (7 days) the elastic properties do not experience a relevant modification [53]; although the strength changes.

The loss of fibre stiffness may be imputed primarily to the dissolution of the component which is responsible for holding the fibrils together (i.e. lignin) and in turns, reducing the relative longitudinal movements. This hypothesis was earlier proposed by [24] who intuitively represented this mechanism using the schematic illustration shown in Figure 12(b). As illustrated, the pre-treatment extensively impairs the structure of the fibres by disorganising the cellulose chains. Further evidence of this mechanism was also seen using SAXS experiment [29] which mainly imputed the fibrils separation to the swelling induced by the presence of the alkaline solution.

5.3. Crystallinity Index and crystal orientation modification

Analysis of the crystallinity change was performed using the Crystallinity Index and the trend is reported in Figure 10(a). However no evidence of relevant change in crystallinity was observed. The maximum variation observed was ~5%, which lies in the 95% confidence interval of a single evaluated point and is therefore without any significance. Concerning the preferential orientation analysis, Figure 10(b) shows an increasing preferred orientation of the $\langle 004 \rangle$ peak. This may be associated with the gradual loss of a less ordered constituent present in the fibres, which in turns become either amorphous or change orientation with respect to the x-ray beam orientation. According to what discussed earlier, the lignin is the constituents that tends to vanish as the alkalinity of the solution exceeds 20%, therefore it is very likely that it is indeed this different form of cellulose that turns its structure into a different crystalline state or maybe even becomes amorphous.

5.4. Deformation by SAXS method and general discussion

As exploited by Cameron [54], the SAXS technique can be employed for the analysis of fibre swelling and associated voids volume fraction increase in the case of native cellulose fibres treated with NaOH. In this work, the variation of the scatter intensity associated to the longitudinal loading direction was monitored. This intensity is proportional to the amount of scattered produced by surfaces lying perpendicular to the loading direction. As expected, as the tensile load was applied to the sample, these surfaces were subject to reduction in area due to the Poisson effect and therefore a decrement of the SAXS intensity was experienced. As illustrated in Figure 11(b), as the load is incrementally applied to the sample, the SAXS intensity decreases following a similar slope for the untreated sample and those samples treated with 5%, 10%, 15% and 20% NaOH solutions. On the other hand, the sample treated with 25% NaOH shows a marked dissimilar behaviour. This behaviour qualitatively resembles the strain behaviour seen from macro tensile stage, WAXS and DIC for stresses up to ~100MPa. Above this value, the samples treated with NaOH <25% do not experience any change in intensity. This may be associated with the inelastic deformation taking place in the bamboo matrix which is not able to withstand a certain amount of stress. It is also worth reporting a recent work which reports an alteration of the fracture behaviour of bamboo when the water content is modified [55]. Hence, the water content in the alkaline solution used in the present work may have contributed in modifying the bamboo toughness experienced. This aspect of the material behaviour is of great importance when dealing with the structural integrity of most of brittle engineering components. In fact, in some cases the overall ductility of the composite is mimicked by designing materials with less strong matrix, which gradually fails earlier than the fibres and enables larger deformations of the overall composite. Large deformations means that a wider margin of safety is guaranteed until the engineering component fails catastrophically. For this reason, the effect of alkaline solution treatment, as well as the related cracking behaviour of the bamboo matrix, plays a key role on the material performance which is surely worth further investigation.

6. Conclusions

The combination of in-situ Synchrotron-based techniques and an optical method has allowed the detailed analysis of the elastic properties modification, and its nature, induced by NaOH treatments. Overall, all the techniques employed confirmed that the elastic modulus of bamboo fibres experiences a gradual increase when the treating solution presents degree of alkalinity up to 20% NaOH. In fact, at 20% NaOH, the increment of

stiffness was assessed of 59% with the respect to the pristine materials. On the other hand, the 25% NaOH solution reduced the elastic modulus of 37%, again with the respect of the pristine material.

As far as the Synchrotron-based techniques are concerned, it has been shown that the analysis of the bamboo constituent's deformation could be conducted by monitoring the lattice size change. In fact, the peak associated with the crystalline plane $\langle 004 \rangle$ clearly provided a quantitative evaluation of the strain taking place in the fibres of the bamboo. While, the $\langle 200 \rangle$ peak is associated to a less ordered system (matrix), given by the broadening effect experienced by this diffraction peak. A confirmation of this assumption comes from the evidence that deformation taking place in the matrix does not exceed ~ 0.01 for the samples treated with 5%, 10%, 15% and 20% NaOH, which can only occur in a constituent different than the fibres, i.e. matrix. The fact that the matrix subject to these solutions cannot withstand deformation larger than this value is explained by the cracking occurring in the matrix at a certain load threshold. Corroboration of this phenomenon could be obtained from the SAXS intensity change plot (Figure 6(b)), which shows unchanged values for loads higher than ~ 100 MPa. It can be concluded that, in the first instance the alkaline solution reduced the matrix toughness for solutions up to 20% NaOH. However, on the other hand the toughness is improved when the 25% NaOH solution was employed. Although in minor entity, this effect influences the overall elastic properties of the bamboo.

Regarding the rapid drop of the bamboo mechanical stiffness at 25% NaOH, particularly the DIC analysis has shed some light onto this mechanism. In fact, it was shown that fibres experience a considerable amount shear strain during tensile test, hinting that the alkaline solution has a negative impact on the adhesion between fibrils. As hypothesised by previous researcher, and confirmed here, the high concentration of NaOH disrupted the fibrils bonding, by eliminating the lignin constituent.

Given the wide range of applications of this material, it is surely worth conducting further investigations in this direction.

7. Appendix - Statistical Methods

The evaluation of uncertainty carried forward, during the several calculation steps, was performed by employing the *Error Propagation* theory.

All the quantities reported in the present manuscript were derived from fundamental measurements read from the dedicated devices, or extracted from image processing. Commencing from simplest derived variables, we report below the advancement of error calculation.

The nominal stress acting in the bamboo's cross section was calculated by using the total force F read from the micro tensile stage, exerted on the whole cross section, divided by the measured cross section area A . The error arising upon force reading was assessed to be $\delta_F = \pm 5$ N, while that of the area was $\delta_A \approx \pm 0.025$ mm² depending upon the specific given sample and assuming that the error of linear measurement to be $\delta_{l_0} = \pm 0.01$ mm. Therefore, the error carried by the evaluated stress is:

$$\delta_\sigma = |\sigma| \sqrt{\left(\frac{\delta_F}{F}\right)^2 + \left(\frac{\delta_A}{A}\right)^2} \quad (6)$$

As far as the strain evaluation is concerned, independent error calculations are required, especially since this quantity was obtained using three independent techniques (i.e. tensile stage macro strain, WAXS and DIC), independent error calculations are required.

The macroscopic assessment of strains was performed by exploiting the tensile stage cross head displacement. It is worth reporting that the tensile stage clamps deform themselves during the loading of the sample. Nevertheless, it was verified that its compliance did not affect the strain evaluation, since its effect was much less significant as compared to that of the tested samples. In this case, assuming the nominal gauge length as l_0 and the monitored length extension as l , the cumulative error was calculated as follows:

$$\delta_{\varepsilon_{macro}} = |\varepsilon_{macro}| \sqrt{\left(\frac{\sqrt{(\delta_{l_0})^2 + (\delta_l)^2}}{l - l_0}\right)^2 + \left(\frac{\delta_{l_0}}{l_0}\right)^2} \quad (7)$$

Regarding the calculation of strains obtained by the WAXS technique, the most sensitive evaluation step for the calculation of errors was the fitting of diffraction peaks. In principle, the fitting process also outputs the error associated with the estimated position of the peak in terms of lattice parameter, at 95% confidence level. In the

equation below, the canonical form for strain error calculation is reported, where δ_d is the fitting error. In this case, we neglect any errors associated with the measure of d_0 , as it was chosen to be corresponding to the lattice dimension at the unloaded sample state.

$$\delta_{\varepsilon_{XRD}} = |\varepsilon_{XRD}| \sqrt{\left(\frac{\delta_d}{d-d_0}\right)^2 + \left(\frac{\delta_d}{d}\right)^2} \quad (8)$$

However, such values resulted to be less significant than those found in the macro strain for the great majority of the measured points. Therefore an averaged value of the arising errors associated with this measure was deliberately assumed to be $\delta_{\varepsilon_{XRD}} = 0.0005$.

DIC analysis of strain distribution across the sample surface showed a large fluctuation, particularly regarding the sample subjected to 25% NaOH. In the view of calculating the elastic modulus by properly manipulating the extracted strain fields, averaged values of strains have to be assessed separately for each specific sample and loading condition. It is also worth noting that the punctual error in strain calculation produced by the DIC method is negligible compared with the large scatter experienced in the material itself, therefore, we do not account for this source of error. Since the DIC markers were equidistantly distributed, the average strain value existing on the sample surface is:

$$\overline{\varepsilon_{DIC}} = \frac{1}{n} \sum_{i=1}^n \varepsilon_{DIC,i} \quad (9)$$

where n indicates the number of DIC markers either on the left or right hand side of the acquired frame.

The error associated to the averaging calculation is promptly derived from its standard deviation. Since we assumed the errors representing the 95% confidence intervals, the error band is defined multiplying the standard deviation by z , which in this case is equal to 1.96. Thereby, the arising error is:

$$\delta_{\overline{\varepsilon_{DIC}}} = z \sqrt{\frac{\sum_{i=1}^n (\varepsilon_{DIC,i} - \overline{\varepsilon_{DIC}})^2}{n-1}} \quad (10)$$

The elastic modulus of the bamboo without separation of fibre and matrix contributions is evaluated by performing linear regressions of the Stress vs. Strain curves. This calculation is applied to all the sets of measurements performed. First of all, the standard error associated to each pair of stress-strain point is:

$$e_i = |E_i| \sqrt{\left(\frac{\delta_{\sigma_i}}{\sigma_i}\right)^2 + \left(\frac{\delta_{\varepsilon_i}}{\varepsilon_i}\right)^2} \quad (11)$$

Therefore, the error associated with this regression process is calculated as:

$$\delta_E = \sqrt{\frac{\sum_{i=1}^N \frac{1}{e_i^2}}{\left(\sum_{i=1}^N \frac{x_i^2}{e_i^2}\right) \left(\sum_{i=1}^N \frac{1}{e_i^2}\right) - \left(\sum_{i=1}^N \frac{x_i}{e_i^2}\right)^2}} \quad (12)$$

In this manuscript, we devoted particular attention to the evaluation of the actual stress existing in the bamboo fibres, with the purpose of evaluating their elastic moduli. As described in the main text, the fraction of fibre φ_f in each analysed sample was evaluated through an optical method, which inherently gives rise to errors. This error was estimated to be $\delta_{\varphi_f} = \pm 0.03$.

Therefore, the elastic modulus of the bamboo fibres can be calculated as:

$$\delta_{E_f} = |E_f| \sqrt{\left(\frac{\delta_{E_c}}{E_c}\right)^2 + \left(\frac{\sqrt{(\delta_{\varphi_f})^2 + (\delta_{f^*})^2}}{\varphi_f + \left(\frac{1-\varphi_f}{\beta}\right)}\right)^2} \quad (13)$$

where δ_{f^*} is the error contained in the denominator of the E_c formulation, which is:

$$\delta_{f^*} = \sqrt{\left(\frac{\delta_{\varphi_f}}{\varphi_f}\right)^2 + \left(\frac{\delta_{\beta}}{\beta}\right)^2} \quad (14)$$

The uncertainty in the exact value of the parameter β is assumed to be $\delta_{\beta} = \pm 9$, according to the considerations described earlier.

Following the above described calculation framework, the estimation of errors was performed for each used technique, and the error bars indicated in the reported figures, refer to the 95% confidence interval.

References

- [1] N.M. Pugno, F. Bosia, T. Abdalrahman, Hierarchical fiber bundle model to investigate the complex architectures of biological materials, *Physical Review E - Statistical, Nonlinear, and Soft Matter Physics* 85(1) (2012).
- [2] J. Guo, J. Tang, Y. Wen, J.L. Zhang, Y.S. Li, Development status of modern bamboo structure building, *Applied Mechanics and Materials*, 2013, pp. 26-29.
- [3] B. Sharma, A. Gatóo, M. Bock, M. Ramage, Engineered bamboo for structural applications, *Construction and Building Materials* 81(Supplement C) (2015) 66-73.
- [4] M.M. Thwe, K. Liao, Effects of environmental aging on the mechanical properties of bamboo-glass fiber reinforced polymer matrix hybrid composites, *Composites - Part A: Applied Science and Manufacturing* 33(1) (2002) 43-52.
- [5] H.P.S. Abdul Khalil, I.U.H. Bhat, M. Jawaid, A. Zaidon, D. Hermawan, Y.S. Hadi, Bamboo fibre reinforced biocomposites: A review, *Materials and Design* 42 (2012) 353-368.
- [6] K. Ghavami, Bamboo as reinforcement in structural concrete elements, *Cement and Concrete Composites* 27(6) (2005) 637-649.
- [7] S. Askarinejad, P. Kotowski, F. Shalchy, N. Rahbar, Effects of humidity on shear behavior of bamboo, *Theoretical and Applied Mechanics Letters* 5(6) (2015) 236-243.
- [8] I.M. Low, Z.Y. Che, B.A. Latella, Mapping the structure, composition and mechanical properties of bamboo, *Journal of Materials Research* 21(8) (2006) 1969-1976.
- [9] S. Amada, T. Munekata, Y. Nagase, Y. Ichikawa, A. Kirigai, Y. Zhifei, The mechanical structures of bamboos in viewpoint of functionally gradient and composite materials, *Journal of Composite Materials* 30(7) (1996) 800-819.
- [10] A.K. Ray, S. Mondal, S.K. Das, P. Ramachandrarao, Bamboo—A functionally graded composite-correlation between microstructure and mechanical strength, *Journal of Materials Science* 40(19) (2005) 5249-5253.
- [11] K. Abe, H. Yano, Comparison of the characteristics of cellulose microfibril aggregates isolated from fiber and parenchyma cells of Moso bamboo (*Phyllostachys pubescens*), *Cellulose* 17(2) (2010) 271-277.
- [12] S. Youssefian, N. Rahbar, Molecular origin of strength and stiffness in bamboo fibrils, *Scientific Reports* 5 (2015).
- [13] A. Bergander, L. Salmén, Cell wall properties and their effects on the mechanical properties of fibers, *Journal of Materials Science* 37(1) (2002) 151-156.
- [14] P. Eronen, M. Österberg, A.S. Jääskeläinen, Effect of alkaline treatment on cellulose supramolecular structure studied with combined confocal Raman spectroscopy and atomic force microscopy, *Cellulose* 16(2) (2009) 167-178.
- [15] M.K. Habibi, Y. Lu, Crack propagation in bamboo's hierarchical cellular structure, *Scientific Reports* 4 (2014).
- [16] J.Q. Krause, F. de Andrade Silva, K. Ghavami, O.D.F.M. Gomes, R.D.T. Filho, On the influence of *Dendrocalamus giganteus* bamboo microstructure on its mechanical behavior, *Construction and Building Materials* 127 (2016) 199-209.
- [17] S. Amada, Y. Ichikawa, T. Munekata, Y. Nagase, H. Shimizu, Fiber texture and mechanical graded structure of bamboo, *Composites Part B: Engineering* 28(1) (1997) 13-20.
- [18] L. Shang, Z. Sun, X. Liu, Z. Jiang, A novel method for measuring mechanical properties of vascular bundles in moso bamboo, *Journal of Wood Science* 61(6) (2015) 562-568.
- [19] P.G. Dixon, K.E. Semple, A. Kutnar, F.A. Kamke, G.D. Smith, L.J. Gibson, Comparison of the flexural behavior of natural and thermo-hydro-mechanically densified Moso bamboo, *European Journal of Wood and Wood Products* 74(5) (2016) 633-642.
- [20] H. Li, S. Shen, The mechanical properties of bamboo and vascular bundles, *Journal of Materials Research* 26(21) (2011) 2749-2756.
- [21] M. Das, A. Pal, D. Chakraborty, Effects of mercerization of bamboo strips on mechanical properties of unidirectional bamboo-novolac composites, *Journal of Applied Polymer Science* 100(1) (2006) 238-244.
- [22] L.H. Zhang, C.S. Chyang, F. Duan, P.W. Li, S.Y. Chen, Comparison of the thermal behaviors and pollutant emissions of pelletized bamboo combustion in a fluidized bed combustor at different secondary gas injection modes, *Energy* 116 (2016) 306-316.
- [23] Z. Liu, B. Fei, Z. Jiang, X. Liu, Combustion characteristics of bamboo-biochars, *Bioresource Technology* 167 (2014) 94-99.
- [24] N. Mosier, C. Wyman, B. Dale, R. Elander, Y.Y. Lee, M. Holtzapple, M. Ladisch, Features of promising technologies for pretreatment of lignocellulosic biomass, *Bioresource Technology* 96(6) (2005) 673-686.
- [25] Z. Yuan, Y. Wen, N.S. Kapu, Ethanol production from bamboo using mild alkaline pre-extraction followed by alkaline hydrogen peroxide pretreatment, *Bioresource Technology* 247 (2018) 242-249.
- [26] P.T. Vu, Y. Unpaprom, R. Ramaraj, Impact and significance of alkaline-oxidant pretreatment on the enzymatic digestibility of *Sphenoclea zeylanica* for bioethanol production, *Bioresource Technology* 247 (2018) 125-130.

- [27] A.W.T. Owolabi, G. Arniza, W. Wan Daud, A.F.M. Alkharkhi, Effect of alkaline peroxide pre-treatment on microfibrillated cellulose from oil palm fronds rachis amenable for pulp and paper and bio-composite production, *BioResources* 11(2) (2016) 3013-3026.
- [28] P. Martel, J.M. Gould, Cellulose stability and delignification after alkaline hydrogen peroxide treatment of straw, *Journal of Applied Polymer Science* 39(3) (1990) 707-714.
- [29] G. Kellermann, A.F. Craievich, R. Neuenschwander, T.S. Plivelic, Setup for in situ WAXS/SAXS studies of the formation and growth of Bi nanodroplets and the melting of Bi nanocrystals using synchrotron radiation, *Nuclear Instruments and Methods in Physics Research, Section B: Beam Interactions with Materials and Atoms* 199 (2003) 112-116.
- [30] H. Guo, J. Wang, C. Zhou, W. Zhang, Z. Wang, B. Xu, J. Li, Y. Shang, J. De Claville Christiansen, D. Yu, Z. Wu, S. Jiang, Direct investigations of deformation and yield induced structure transitions in polyamide 6 below glass transition temperature with WAXS and SAXS, *Polymer (United Kingdom)* 70 (2015) 109-117.
- [31] B. Gurun, D.G. Bucknall, Y.S. Thio, C.C. Teoh, E. Harkin-Jones, Multiaxial deformation of polyethylene and polyethylene/clay nanocomposites: In situ synchrotron small angle and wide angle X-ray scattering study, *Journal of Polymer Science, Part B: Polymer Physics* 49(9) (2011) 669-677.
- [32] J.C. Viana, J.F. Mano, Z.Z. Denchev, M.J. Oliveira, M.C. Cramez, Nanostructure evolution during uni-axial deformation of PET - A WAXS and SAXS study using synchrotron radiation, *Materials Science Forum*, 2006, pp. 1583-1587.
- [33] T. Sui, E. Salvati, S. Ying, G. Sun, I.P. Dolbnya, K. Dragnevski, C. Prisacariu, A.M. Korsunsky, Strain softening of nano-scale fuzzy interfaces causes Mullins effect in thermoplastic polyurethane, *Scientific Reports* 7(1) (2017).
- [34] T. Sui, N. Baimpas, I.P. Dolbnya, C. Prisacariu, A.M. Korsunsky, Multiple-length-scale deformation analysis in a thermoplastic polyurethane, *Nature Communications* 6 (2015).
- [35] C.S. Gritsch, G. Kleist, R.J. Murphy, Developmental changes in cell wall structure of phloem fibres of the bamboo *Dendrocalamus asper*, *Annals of Botany* 94(4) (2004) 497-505.
- [36] J. Bolze, J. Kim, J.Y. Huang, S. Rah, H.S. Youn, B. Lee, T.J. Shin, M. Ree, Current status of the synchrotron small-angle X-ray scattering station BL4C1 at the Pohang Accelerator Laboratory, *Macromolecular Research* 10(1) (2002) 2-12.
- [37] A. Hedberg-Buenz, M.A. Christopher, C.J. Lewis, K.J. Meyer, D.S. Rudd, L.M. Dutca, K. Wang, M.K. Garvin, T.E. Scheetz, M.D. Abramoff, M.M. Harper, M.G. Anderson, RetFM-J, an ImageJ-based module for automated counting and quantifying features of nuclei in retinal whole-mounts, *Experimental Eye Research* 146 (2016) 386-392.
- [38] E. Salvati, A.J.G. Lunt, S. Ying, T. Sui, H.J. Zhang, C. Heason, G. Baxter, A. Korsunsky, Eigenstrain Reconstruction of Residual Strains in an Additively Manufactured and Shot Peened Nickel Superalloy Compressor Blade, *Computer Methods in Applied Mechanics and Engineering* (2017).
- [39] E. Salvati, H. Zhang, K.S. Fong, X. Song, A.M. Korsunsky, Separating plasticity-induced closure and residual stress contributions to fatigue crack retardation following an overload, *Journal of the Mechanics and Physics of Solids* 98 (2017) 222-235.
- [40] E. Salvati, T. Sui, H. Zhang, A.J.G. Lunt, K.S. Fong, X. Song, A.M. Korsunsky, Elucidating the Mechanism of Fatigue Crack Acceleration Following the Occurrence of an Underload Advanced Engineering Material, (2016).
- [41] J. Holmberg, A. Steuwer, A. Stormvinter, H. Kristoffersen, M. Haakanen, J. Berglund, Residual stress state in an induction hardened steel bar determined by synchrotron- and neutron diffraction compared to results from lab-XRD, *Materials Science and Engineering A* 667 (2016) 199-207.
- [42] A.M. Korsunsky, G.M. Regino, D.P. Latham, H.Y. Li, M.J. Walsh, Residual stresses in rolled and machined nickel alloy plates: Synchrotron X-ray diffraction measurement and three-dimensional eigenstrain analysis, *Journal of Strain Analysis for Engineering Design* 42(1) (2007) 1-12.
- [43] T.-S. Jun, A.M. Venter, A.M. Korsunsky, Inverse Eigenstrain Analysis of the Effect of Non-uniform Sample Shape on the Residual Stress Due to Shot Peening, *Experimental Mechanics* 51(2) (2011) 165-174.
- [44] N. Schalk, J. Keckes, C. Czettl, M. Burghammer, M. Penoy, C. Michotte, C. Mitterer, Investigation of the origin of compressive residual stress in CVD TiB₂ hard coatings using synchrotron X-ray nanodiffraction, *Surface and Coatings Technology* 258 (2014) 121-126.
- [45] S. Park, J.O. Baker, M.E. Himmel, P.A. Parilla, D.K. Johnson, Cellulose crystallinity index: Measurement techniques and their impact on interpreting cellulase performance, *Biotechnology for Biofuels* 3 (2010).
- [46] M. Senn, Digital Image Correlation and Tracking, [Computer Software] <https://uk.mathworks.com/matlabcentral/fileexchange/50994-digital-image-correlation-and-tracking> (2015).
- [47] Z.-P. Shao, C.-H. Fang, S.-X. Huang, G.-L. Tian, Tensile properties of Moso bamboo (*Phyllostachys pubescens*) and its components with respect to its fiber-reinforced composite structure, *Wood Science and Technology* 44(4) (2010) 655-666.
- [48] S. Eyley, W. Thielemans, Surface modification of cellulose nanocrystals, *Nanoscale* 6(14) (2014) 7764-7779.
- [49] K.O. Mohini Sain, Aji P Mathew, Alexander Bismarck;Orlando Rojas;Mohini Sain, Orlando Rojas, Handbook Of Green Materials: Processing Technologies, Properties And Applications (In 4 Volumes), WSPC (2014).
- [50] J.Y. Li, X.M. Ye, J.X. Yu, L.L. Cai, S.M. Ruan, Z.Z. Chang, Study on the rice straw pretreated with NaOH for biogasification, *Advanced Materials Research*, 2011, pp. 140-146.
- [51] T. Tanimoto, T. Nakano, Stress relaxation of wood partially non-crystallized using aqueous NaOH solutions, *Carbohydrate Polymers* 87(3) (2012) 2145-2148.
- [52] M. Das, D. Chakraborty, Evaluation of improvement of physical and mechanical properties of bamboo fibers due to alkali treatment, *Journal of Applied Polymer Science* 107(1) (2008) 522-527.
- [53] Q. Xu, K. Harries, X. Li, Q. Liu, J. Gottron, Mechanical properties of structural bamboo following immersion in water, *Engineering Structures* 81 (2014) 230-239.

- [54] R.E. Cameron, J. Crawshaw, G.R. Mant, W. Bras, Simultaneous SAXS and WAXS investigations of changes in native cellulose fiber microstructure on swelling in aqueous sodium hydroxide, *Journal of Applied Polymer Science* 83(6) (2002) 1209-1218.
- [55] G. Chen, H. Luo, S. Wu, J. Guan, J. Luo, T. Zhao, Flexural deformation and fracture behaviors of bamboo with gradient hierarchical fibrous structure and water content, *Composites Science and Technology* 157 (2018) 126-133.